

An elasto-plastic damage constitutive model for jointed rock mass with an application

Hanpeng Wang^{1a}, Yong Li^{*1,2}, Shucaï Li^{1b}, Qingsong Zhang^{1c} and Jian Liu^{2d}

¹ Geotechnical & Structural Engineering Research Center, Shandong University,
No. 17923 Jingshi Rd., Jinan, Shandong Province, P.R. China 250061

² School of Civil Engineering, Shandong University,
No. 17922 Jingshi Rd., Jinan, Shandong Province, P.R. China 250061

(Received December 07, 2015, Revised March 20, 2016, Accepted March 22, 2016)

Abstract. A forked tunnel, as a special complicated underground structure, is composed of big-arch tunnel, multi-arch tunnel, neighborhood tunnels and separate tunnels according to the different distances between two separate tunnels. Due to the complicated process of design and construction, surrounding jointed rock mass stability of the big-arch tunnel which belongs to the forked tunnel during excavation is a hot issue that needs special attentions. In this paper, an elasto-plastic damage constitutive model for jointed rock mass is proposed based on the coupling method considering elasto-plastic and damage theories, and the irreversible thermodynamics theory. Based on this elasto-plastic damage constitutive model, a three dimensional elasto-plastic damage finite element code (D-FEM) is implemented using Visual Fortran language, which can numerically simulate the whole excavation process of underground project and perform the structural stability of the surrounding rock mass. Comparing with a popular commercial computer code, three dimensional fast Lagrangian analysis of continua (FLAC3D), this D-FEM has advantages in terms of rapid computing process, element grouping function and providing more material models. After that, FLAC3D and D-FEM are simultaneously used to perform the structural stability analysis of the surrounding rock mass in the forked tunnel considering three different computing schemes. The final numerical results behave almost consistent using both FLAC3D and D-FEM. But from the point of numerically obtained damage softening areas, the numerical results obtained by D-FEM more closely approach the practical behaviors of in-situ surrounding rock mass.

Keywords: jointed rock mass; forked tunnel; stability analysis; D-FEM; FLAC3D

1. Introduction

Until the end of 2014, the traffic mileage of national highways in China had exceeded 4,463,900 kilometers (Ma *et al.* 2015). With the demand for “western development” (Shih 2004) and the implementation of “one belt and one road” strategy (Liu 2015), more and more

*Corresponding author, Assistant Professor, Ph.D., E-mail: yongli@sdu.edu.cn

^a Associate Professor, E-mail: pcwli@163.com

^b Professor, Ph.D., E-mail: lishucaï@sdu.edu.cn

^c Professor, Ph.D., E-mail: zhangqingsong@sdu.edu.cn

^d Professor, Ph.D., E-mail: lj75@sdu.edu.cn

underground highway tunnels will be built in western areas in China. From the official statistical data, there had been 11,359 highway tunnels with a total mileage of 9,605.6 kilometers until the end of 2013 (Hong 2015). In the western regions with high mountains and gorges, it is inevitable to adopt a forked structure for the design of highway tunnels so that fewer bridges across the valleys would be invested. A forked tunnel, as a special complicated underground structure, is composed of big-arch tunnel, multi-arch tunnel, neighborhood tunnels and separate tunnels according to the different distances between two separate tunnels as shown in Fig. 1. A number of related research works on crossing tunnels and bifurcated tunnels have been investigated by previous researchers (Liu *et al.* 2009, Ng *et al.* 2013, Lin *et al.* 2013) As for this special complicated structure, the related investigations on the construction sequence, stress and deformation analysis, and surrounding rock mass stability analysis are still in a preliminary stage. Therefore, the authors will attempt to perform numerical investigations on the surrounding rock mass stability of the forked tunnel.

The naturally existing rock mass is the basis of the actual underground infrastructure projects. Under the long-term geological functions, the natural rock mass has crucial property of being incised by all types of discontinuities such as faults, joints, fractures and so forth (Li *et al.* 2015). These structural planes, to some extent, can remarkably reduce the strengths of rock mass, absolutely including the physico-mechanical parameters of jointed rock mass (Li *et al.* 2014). Moreover, the in-situ stress in the underground projects cannot be neglected as it can result in the generations of numerous micro-and meso-cracks in the process of deep excavations (Zhu *et al.* 2011, Lin *et al.* 2015). With the increasing of the external loads, these cracks would gradually extend and even propagate (Hoek and Bieniawski 1965, Bombolakis 1968, Lee and Jeon 2011, Haeri *et al.* 2014). This kind of crack extension and propagation can be regarded as the damage behavior in the surrounding rock mass. The initiation of damage behavior in the surrounding rock mass has also been investigated. Some field experiments were conducted to determine the excavation disturbed zone (EDZ) in Neogene sedimentary rock at Tono mine, central Japan (Sato *et al.* 2000). A mini-sonic borehole probe was performed to investigate the EDZ around an underground opening in the Opalinus Clay in the Mont Terri Rock Laboratory in Switzerland (Schuster *et al.* 2001). Sheng *et al.* (2002) utilized the displacement monitoring, plate loading and

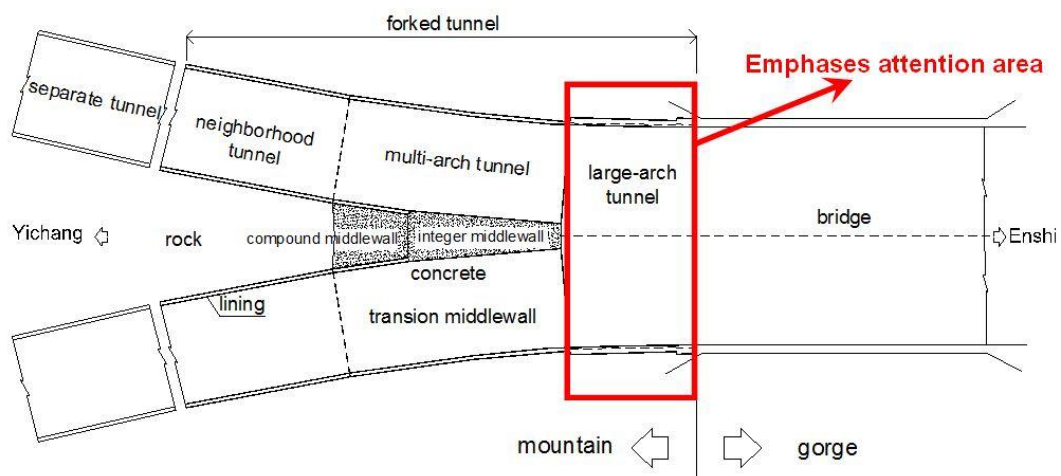


Fig. 1 Component parts of a forked tunnel

seismic tests, cross-hole acoustic and seismic wave penetration testing and drill-hole deformation testing to estimate the EDZ in the slopes of the Three Gorges Project, China. Kruschwitz and Yaramanci (2004) evaluated the specification and monitoring of the EDZ with application of the complex resistivity method in a tunnel project in Switzerland. Cai and Kaiser (2005) studied the quantification of damage degree and the extent of EDZ around underground opening using a micromechanics model based on the acoustic emission and microseismic events. Wu *et al.* (2009) proposed a new method to quantify the extent and damage degree of the EDZ based on the unloading strain energy. Wang *et al.* (2015) made an assessment of the EDZ around roadways under dynamic pressure. Obviously, the former investigators studied EDZ most from the in-situ test results which were high in cost and difficult to implement. During the prophase research work of a significant engineering project, establishing a numerical model and performing numerical simulation is quite an efficient method. Therefore, the authors would like to propose an elasto-plastic damage constitutive model for jointed rock mass in this paper.

As for the development of elasto-plastic damage constitutive model, it was firstly proposed by Kachanov (1958) and then it could be named as continuum damage mechanics (CDM). And the basic concepts and definitions of CDM were detailedly introduced by Krajcinovic (1985). Voyiadjis and Park (1999) presented an elasto-plastic damage model based on the principles of irreversible thermodynamics and finite element method. Zhu *et al.* (2003) put forward a brittle damage constitutive model for jointed rock mass and used it to perform the stability analysis of the high slopes of ship lock of Three Gorges Project being under construction. Chen *et al.* (2004) proposed a damage coupled time-dependent model for jointed rock mass and successfully used it in the stability analysis of a large-scale underground cavern group. Liu and Yuan (2014) also presented a damage constitutive model for jointed rock mass considering micro-cracks, joints and joint shear strength. It can be easily understood that the above-mentioned works are either insufficient in the engineering application or only valid in some rock specimens with special flaws. In this manuscript, an elasto-plastic damage constitutive model for jointed rock mass is proposed based on the coupling method considering elasto-plastic and damage theories, and the irreversible thermodynamics theory. And then, on a basis of this elasto-plastic damage constitutive model, a three dimensional elasto-plastic damage finite element code (D-FEM) is implemented using VISUAL FORTRAN language. Eventually, this D-FEM code would be applied to perform a stability analysis on a forked tunnel during excavation.

2. Elasto-plastic damage constitutive model for jointed rock mass

2.1 Elasto-plastic damage model

Owing to the consideration of the damage behavior in jointed rock mass, here the total strain ε is divided into three parts: elastic strain ε^e , plastic strain ε^p and damage strain ε^d . The damage strain is generated during the elasto-plastic stage of jointed rock mass. The total stress-strain relationship for jointed rock mass under the uniaxial stress state is shown in Fig. 2. In Fig. 2, ε^f denotes the threshold of damage strain. When the strain of the rock mass is smaller than this threshold, it can be considered that no damage occurs in the rock mass and the elasticity modulus would keep constant. The unloading stress route will return along the original stress route. When the strain of the rock mass is greater than the threshold of damage strain, it can be regarded that damage caused by internal micro-cracks has occurred, the corresponding elasticity modulus will be

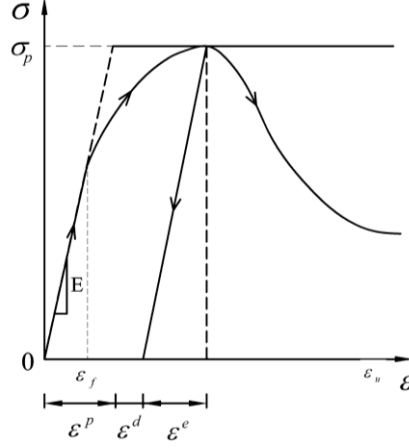


Fig. 2 Elasto-plastic damage stress-strain curve for the uniaxial state of stress

reduced, and only the elastic strain can be recovered during the unloading state. After the stress is up to the peak strength, the stress would decrease with the increasing of the strain until the ultimate strain (ε^u) is achieved. Therefore, according to the irreversible thermodynamics theory (Voyiadjis *et al.* 1999), the total strain rate of the jointed rock mass can be expressed as below

$$\dot{\varepsilon} = \dot{\varepsilon}^e + \dot{\varepsilon}^d + \dot{\varepsilon}^p = C^{e-d} : \dot{\sigma} + \dot{C}^{e-d} : \sigma + \dot{\varepsilon}^p \quad (1)$$

here, $\dot{\varepsilon}$ denotes the total strain rate of jointed rock mass; $\dot{\varepsilon}^e = C^{e-d} : \dot{\sigma}$ denotes the elastic strain rate of jointed rock mass in a certain damaged state; C^{e-d} denotes the elastic damage flexibility tensor; $\dot{\varepsilon}^p = \dot{\lambda} \frac{\partial F}{\partial \sigma}$ denotes the plastic strain rate, λ is the plastic multiplier and F denotes yield functions of different yield criteria; $\dot{\varepsilon}^d = \dot{C}^{e-d} : \sigma$ is additional coupling strain rate induced by the deterioration effect of the jointed rock mass (this is the so called damage evolution coupling strain rate).

As the elastic damage flexibility tensor C^{e-d} can be written as

$$C^{e-d} = C^e + C^d \quad (2)$$

here the elastic flexibility C^e is a constant, therefore Eq. (2) can be expressed as the incremental form

$$\dot{C}^{e-d} = \dot{C}^d \quad (3)$$

finally, the elasto-plastic damage constitutive model can be established as below

$$\dot{\varepsilon}^d = \dot{C}^d : \sigma \quad (4)$$

2.2 Damage evolution equation

As we know, the damage evolution equation is the criterion which can describe the relationship between damage variable, stress and strain. Once the geo-materials enter the damage state, the

damages elements would gradually evolve with the variations of stress and strain. The damage process is absolutely irreversible.

Former researchers have established different damage evolution equations. The two typical damage evolution equations are described as below:

- Qin (2001) presented that the damage variable of jointed rock mass is proportional to external force work, and the damage evolution equation of geo-material can be deduced as below

$$D = 1 - \exp\left(-\frac{E_0}{2Y}\varepsilon^2\right) \quad (5)$$

where E_0 is the initial elasticity modulus, and Y represents the material constant which is equal to the ratio of external force work and damage variable.

- Tang (1997) established a damage statistical constitutive model based on Weibull distribution (Weibull 1951, Keats and Lawrence 1997). It was assumed that the strength of mesoscopic elements followed the Weibull distribution function as following

$$P(\varepsilon) = \begin{cases} \frac{m}{F_0} \left(\frac{\varepsilon}{F_0}\right)^{m-1} \exp\left[-\left(\frac{\varepsilon}{F_0}\right)^m\right], & \varepsilon > 0 \\ 0, & \varepsilon \leq 0 \end{cases} \quad (6)$$

where F_0 and m represent distribution parameters; m is a homogeneous index of geo-material which can measure the concentration of ε ; and $P(\varepsilon)$ is the percentage of damaged elements out of the total number of the mesoscopic elements in rock (Tang 1997). Finally, the damage evolution equation of mesoscopic for the rock mass can be expressed as below

$$D = 1 - \exp\left[-\left(\frac{\varepsilon}{F_0}\right)^m\right] \quad (7)$$

But in this paper, the authors consider that the controlling factor of damage evolution is strain which can be conveniently obtained from the laboratory experiment, the relationship between damage variable and strain can be expressed as following

$$D = \varphi(\varepsilon_{ij}) \quad (8)$$

where φ denotes the function symbol. And the incremental form of Eq. (8) is

$$dD = \frac{\partial \varphi(\varepsilon_{ij})}{\partial \varepsilon_{ij}} d\varepsilon_{ij} \quad (9)$$

According to the definition of threshold of damage strain, the following equations would be satisfied

$$D = \varphi(\varepsilon_u) = 0, \quad D = \varphi(\varepsilon_f) = 1 \quad (10)$$

In Eqs. (10), ε_u and ε_f can be both obtained from laboratory experiments. As for the geo-materials, the damage threshold under the compressive stress state is always not equal to that under the tensile stress state. Based on the Eqs. (8)-(10), the damage evolution equation under uniaxial stress state can be expressed as below

$$D = \begin{cases} 0, & (0 < \varepsilon \leq \varepsilon_f) \\ \frac{\varepsilon_u(\varepsilon - \varepsilon_f)}{\varepsilon(\varepsilon_u - \varepsilon_f)}, & (\varepsilon_f < \varepsilon < \varepsilon_u) \end{cases} \quad (11)$$

According to Mazars and Pijaudier-Cabot' method (1989), the tensile strain ε_t and the compressive strain ε_c could be substituted by equivalent tensile strain $\bar{\varepsilon}_t$ and equivalent compressive strain $\bar{\varepsilon}_c$ in three dimensional conditions. The equivalent tensile and compressive strains are shown in the following equations

$$\bar{\varepsilon}_t = \sqrt{(\varepsilon_1)^2 + (\varepsilon_2)^2 + (\varepsilon_3)^2}, \quad \bar{\varepsilon}_c = \sqrt{\langle -\varepsilon_1 \rangle^2 + \langle -\varepsilon_2 \rangle^2 + \langle -\varepsilon_3 \rangle^2} \quad (12)$$

here ε_1 , ε_2 and ε_3 denote the three principal strains; the symbol $\langle x \rangle$ denotes a function which has a definition as $\langle x \rangle = \begin{cases} x, & x \geq 0 \\ 0, & x < 0 \end{cases}$.

When the compressive and tensile principal stresses simultaneously exist in the element, the total damage variable would be the sum of the damage variable caused by uniaxial tension (D_t) and the damage variable caused by uniaxial compression (D_c) as expressed below

$$D = \alpha_t D_t + \alpha_c D_c \quad (13)$$

where α_t and α_c are combination coefficients which can be determined as the following equation

$$\begin{cases} \alpha_t = \sum_i \frac{\varepsilon_{Ti}(\varepsilon_{Ti} + \varepsilon_{Ci})}{\bar{\varepsilon}^2} \\ \alpha_c = \sum_i \frac{\varepsilon_{Ci}(\varepsilon_{Ti} + \varepsilon_{Ci})}{\bar{\varepsilon}^2} \end{cases} \quad (14)$$

where ε_{Ti} represents the strain caused by positive principal stress; ε_{Ci} represents the strain caused by negative principal stress; $\bar{\varepsilon}$ is the equivalent strain. Consequently, the damage evolution equations in the elasto-plastic damage constitutive model have been proposed in this part.

2.3 Additional load caused by damage

Here, we define σ_{ij} as the stress of geo-material considering the damage behavior, and define σ_{ij}^0 as that without considering the damage behavior. The relationship between σ_{ij} and σ_{ij}^0 can be expressed as below

$$\sigma_{ij} = (1 - D)\sigma_{ij}^0 + \frac{D}{3}\delta_{ij}\sigma_{ij}^0 \quad (15)$$

Substituting $\sigma_{ij}^0 = E_{ijkl}\varepsilon_{kl}$ into Eq. (15), we will obtain a following matrix form

$$\sigma = \bar{E}\varepsilon = \begin{bmatrix} B & A & A & 0 & 0 & 0 \\ A & B & A & 0 & 0 & 0 \\ A & A & B & 0 & 0 & 0 \\ 0 & 0 & 0 & C & 0 & 0 \\ 0 & 0 & 0 & 0 & C & 0 \\ 0 & 0 & 0 & 0 & 0 & C \end{bmatrix} \varepsilon \quad (16)$$

where $A = \frac{E\mu}{(1+\mu)(1-2\mu)} + \frac{E}{1+\mu} \cdot \frac{D}{3}$; $B = \frac{E(1-\mu)}{(1+\mu)(1-2\mu)} - \frac{E}{1+\mu} \cdot \frac{2D}{3}$; $C = \frac{E}{2(1+\mu)} \cdot (1-D)$; μ denotes the Poisson's ratio of geo-material.

It can be obviously known from Eq. (1) that the additional load caused by damage is related to the increment of damage stiffness matrix. Therefore, to obtain the additional load caused by damage, we have to obtain the increment of damage stiffness matrix. Calculating the derivative of Eq. (16), the increment of the damage stiffness matrix can be obtained as below

$$\Delta \bar{E} = \frac{\partial \bar{E}}{\partial D} \cdot \Delta D = \begin{bmatrix} B' & A' & A' & 0 & 0 & 0 \\ A' & B' & A' & 0 & 0 & 0 \\ A' & A' & B' & 0 & 0 & 0 \\ 0 & 0 & 0 & C' & 0 & 0 \\ 0 & 0 & 0 & 0 & C' & 0 \\ 0 & 0 & 0 & 0 & 0 & C' \end{bmatrix} \cdot \Delta D \quad (17)$$

where $A' = \frac{E}{3(1+\mu)}$; $B' = -\frac{2E}{3(1+\mu)}$; $C' = -\frac{E}{2(1+\mu)}$.

The additional load would be generated once an element is damaged, and the additional nodal force would be generated simultaneously. In order to satisfy the structural equilibrium principle, the additional nodal force should be integrated into the load vectors. Therefore, the additional force caused by damage evolution ($\{F_d\}$) can be calculated according the following equation

$$\{F_d\} = - \iiint [B]^T [\Delta D] \{\varepsilon\} dV \quad (18)$$

3. Implementation of three dimensional D-FEM code

As the additional force caused by damage evolution must be taken into account, the virtual work of the additional force should be also considered in virtual work equation of the finite element method. According to the virtual work principle, the finite element equations of integral structure considering damage behavior can be expressed as below

$$[K]_{ij} \{\delta\}_j = \{F\}_i + \{F_d\}_i \quad (19)$$

where $[K]_{ij}$ denotes the stiffness matrix; $\{\delta\}_j$ denotes the displacement matrix of the nodes; $\{F\}_i$ denotes the equivalent node load vector. According to Eq. (19), the corresponding three dimensional D-FEM code can be written using Visual Fortran language. The program flow chart of D-FEM is show in the following Fig. 3.

Meanwhile, the interface programs of pre-processing and post-processing are also compiled. The pre-processing interface program can read the nodal information of three dimensional isoparametric elements so as to generate any complex numerical models. The post-processing interface program can deal with the numerical results and make them visualization using the Tecplot software (Tecplot Inc. 2013). Therefore, the D-FEM code proposed above has the following advanced functions:

- It can simulate elastic, elasto-plastic, elastic damage and even elasto-plastic damage problems in geo-materials. It can provide different plastic constitutive models including

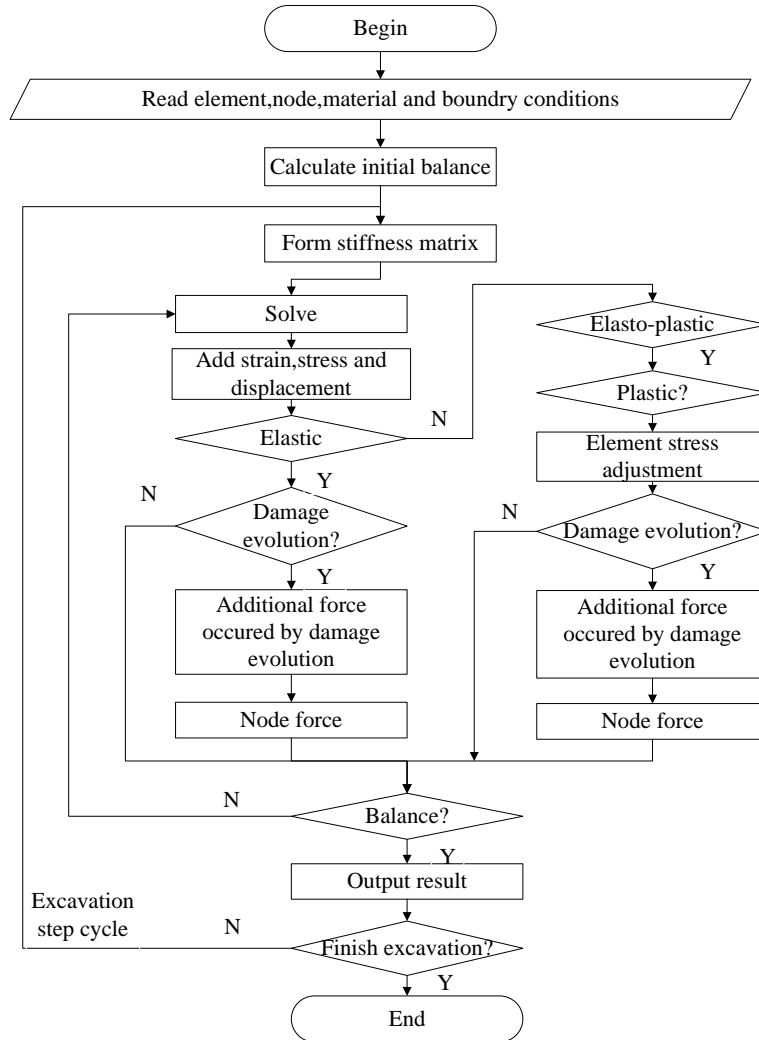


Fig. 3 A program flow chart of D-FEM

Tresca model (Taiebat *et al.* 2008), von Mises model (Leu 2005), Drucker-Prager model (Drucker and Prager 1953), Mohr-Coulomb model (Singh and Singh 2012) and Zienkiewicz-Pande model (Zienkiewicz *et al.* 1980), which are more than those FLAC3D and other commercial codes provide;

- It can provide tetrahedron, pentahedron and hexahedron isoparametric elements and read information files of node, element and material property, so any complex geometry model can be generated;
- It has an “element birth and death” module and can simulate excavation and support in engineering construction process by means of modifying elements’ mechanical parameters;
- It has group function, namely that some elements can be partitioned as the same group, it can operate comfortably and effectively like FLAC3D;
- Preconditions conjugate gradient method is adopted in the program iterative solution, which

can be applied to solve nonlinear problems more efficiently than FLAC3D;

- The post-processing interface program can be used to make the numerical results visualization using Tecplot, which has better effects in generating all kinds of contours than FLAC3D.

4. Verification of the D-FEM code and engineering application

4.1 Project description

A forked tunnel project is located in the city of Enshi, Hubei province, China. It belongs to a part of the highway from Shanghai to Chengdu. The rock mass at the forked tunnel site mainly consists of microcrystalline limestone (T_{1d}^2) and shaly limestone (P_{1q}). Field tests reveal that the in-situ stress field of the tunnel site is a combination of the self-stress field and the tectonic stress field with complex geological conditions. The natural gradient of the rock slope nearby is 40-60°. Due to the limitations of complex topographic conditions, a special forked tunnel is designed. Two separated tunnels are designed at the entrance and a big-arched tunnel is designed at the exit. The transitional section from the big-arch tunnel to two separated tunnels is named a multiple-arch tunnel. The different segmentations of tunnel sections are shown in Fig. 1.

From the construction difficulties of the forked tunnel, the big-arch tunnel is considered to be the most difficult. Therefore, the whole construction process stability analysis of the big-arch tunnel is determined to be mainly investigated.

4.2 Numerical model of the big-arch tunnel

The upper-lower bench method is adopted in the excavations of the big-arch tunnel as shown in Fig. 4. The upper bench is firstly excavated, and then the lower bench is excavated. The entire excavation process is divided into 4 steps for the big-arch tunnel. Specifically, the first step includes excavation of I1, followed by the second excavation II1, and so forth at 2 m increments in the big-arch tunnel. The three dimensional numerical model of the big-arch tunnel is established as shown in Fig. 5. The whole numerical model is divided into 6,255 nodes and 4,084 elements. The eight-node hexahedron isoparametric elements are adopted in the numerical model. The upper surface is an unconstrained surface and sliding constraints are applied on other planes. As the in-situ stress in the surrounding rock mass is not big, the self-weight stress is only taken into account in the numerical simulation.

4.3 Calculating schemes

To verify the effectiveness of the D-FEM code, FLAC3D is also adopted in the numerical simulation. The following three calculating schemes are performed:

- Scheme I is an elasto-plastic calculation without considering the damage evolution. In order to verify the effectiveness of D-FEM code, Mohr-Coulomb criterion is adopted in the D-FEM code and then a comparative analysis can be performed with the numerical results obtained by FLAC3D;
- Scheme II adopts the D-FEM code to perform the elasto-plastic damage calculation. The compressive strain threshold takes the value of 0.0005, and the tensile strain threshold takes

the value of 0.0004;

- Scheme III also adopts the D-FEM code to perform the elasto-plastic damage calculation. The compressive strain threshold takes the value of 0.0007, and the tensile strain threshold takes the value of 0.0005;

When FLAC3D is used to make the elasto-plastic calculation, the excavation sequence the physico-mechanical parameters are the same as those adopted in the D-FEM code calculations. The physico-mechanical parameters of surrounding rock mass are shown in Table 1, which are obtained from a report provided by the Second Highway Investigation and Design Institute (SHIDI) of Ministry Of Communication of China (SHIDI 2004).

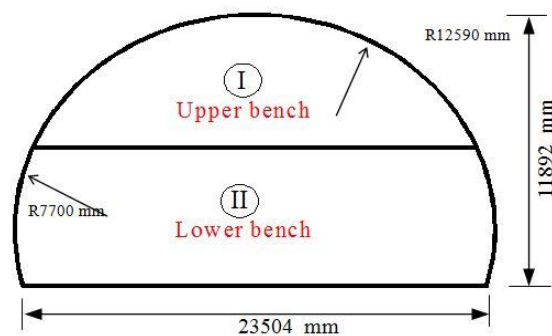


Fig. 4 Excavating sequences for the big-arch tunnel

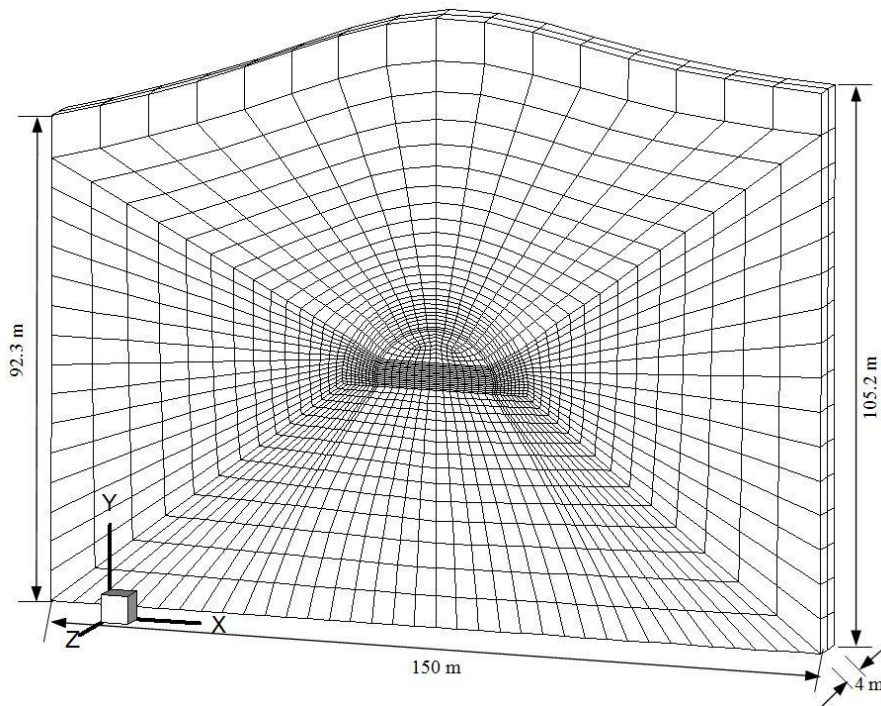


Fig. 5 Three dimensional numerical model of the big-arch tunnel

Table 1 Physico-mechanical parameters of surrounding rock mass

Calculating schemes	Considering damage evolution?	Density (kN/m^3)	Elastic modulus (MPa)	Poisson's ratio (μ)	Cohesion (MPa)	Friction angle ($^\circ$)	Tensile strength (MPa)	Uniaxial compression		Uniaxial tension	
								ε_f	ε_u	ε_f	ε_u
I	NO	27.8	8000	0.22	1.3	40	1.0	0.0005	0.005	0.0004	0.004
II	YES	27.8	8000	0.22	1.3	40	1.0	0.0005	0.005	0.0004	0.004
III	YES	27.8	8000	0.22	1.3	40	1.0	0.0007	0.007	0.0005	0.005

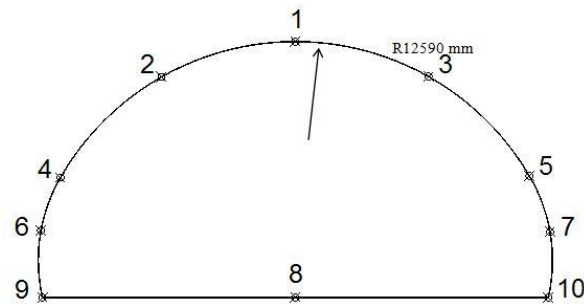


Fig. 6 Selected 10 key points in the surrounding rock mass

4.4 Comparative analysis on the calculating results

4.4.1 Displacement of key points

To make a comparative analysis on the displacement of the surrounding rock mass when the excavation steps are all completed, ten key points are selected as shown in Fig. 6.

The displacements of ten key points have been obtained by performing the three calculating schemes and FLAC3D. Fig. 7 shows the horizontal and vertical displacements of ten key points.

From the displacement comparative curves above, the following conclusions can be drawn:

- The numerical displacements obtained by scheme I is almost in good agreement with those obtained by FLAC3D. The only difference is that the vertical displacement of arch crown obtained by scheme I is a little smaller and the floor shifting is a little larger;
- As the damage evolution is considered in scheme II and III, the vertical displacements of some key points obtained by them are obviously larger than those obtained by scheme I. The vertical displacement of the arch crown increases by 7.1%. Among of them, the displacement variation of key point No. 5 is the most obvious, and the vertical displacement in scheme II is almost twice of that in scheme I;
- As for the horizontal displacement, the horizontal displacements of key points No. 4, No. 5 and No. 7 have obvious variations. The displacement of key point No. 7 decreases by 40%, and even the displacements of key points No. 4 and No. 5 have changed original directions. These local obvious displacement changes are caused by the damage evolution in the surrounding rock mass;
- As for scheme III, the displacement variations are not more obvious than those in scheme II as scheme III adopts a larger damage strain threshold value which results in smaller damages zones.

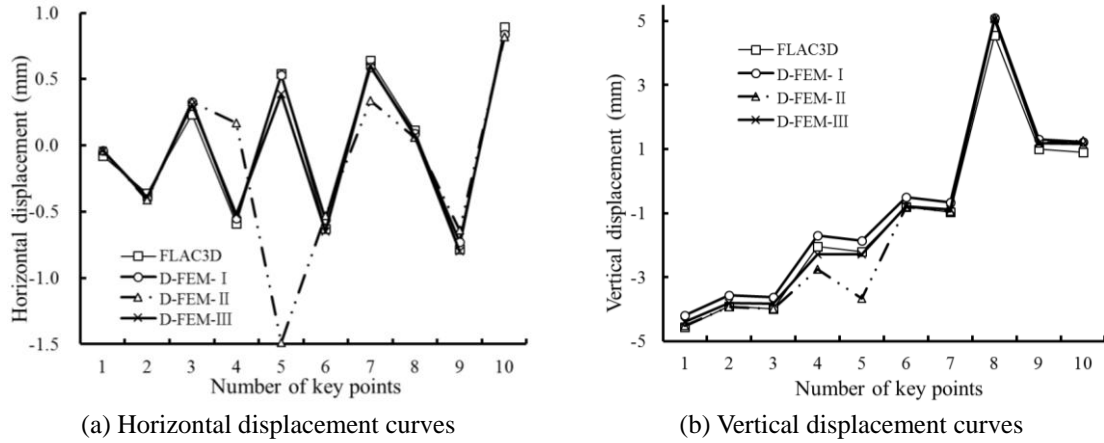


Fig. 7 Comparative curves on the displacements of ten key points in the surrounding rock mass

4.4.2 Stress field

Figs. 8 and 9 show the minimal and maximum principal stress contours obtained by scheme I and FLAC3D. The numerical results show that the principle of stress distribution is almost the same.

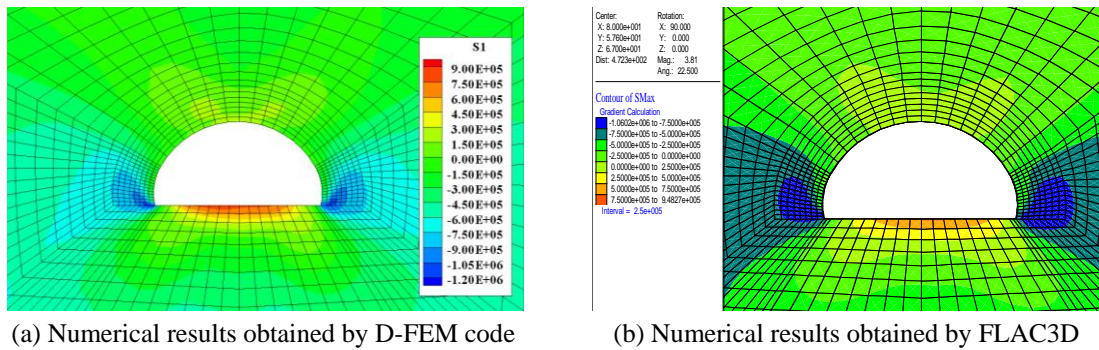


Fig. 8 Minimum principal stress contours obtained by both D-FEM code and FLAC3D

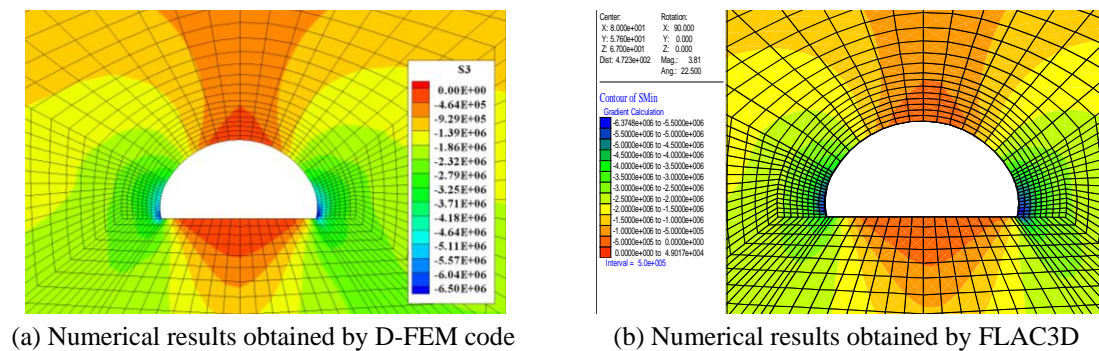


Fig. 9 Maximum principal stress contours obtained by both D-FEM code and FLAC3D

4.4.3 Distribution of damaged zones

When the D-FEM code is used to perform the numerical simulation, the damaged zones would appear in the surrounding rock mass gradually with the excavation steps. The following figures show the damaged zones in schemes I, II and III.

It can be concluded from the above figures on the distribution of damaged zones as below:

- As for schemes I and II, although they adopt the same damage strain threshold and upper-limit strain, the damaged zones in scheme II is obviously larger than those in scheme I as scheme I does not consider the damage evolution process. During the damage evolution process, the damaged elements would release the stress and transfer it to the deeper elements in the surrounding rock mass, which can result in larger damaged zones;
- Comparing scheme III with scheme II, when the damage strain threshold and upper-limit strain are increased, the corresponding damaged zones would become smaller. Therefore, it can be concluded that the physico-mechanical parameters have significant influences on the stability and damage behavior of the surrounding rock mass.

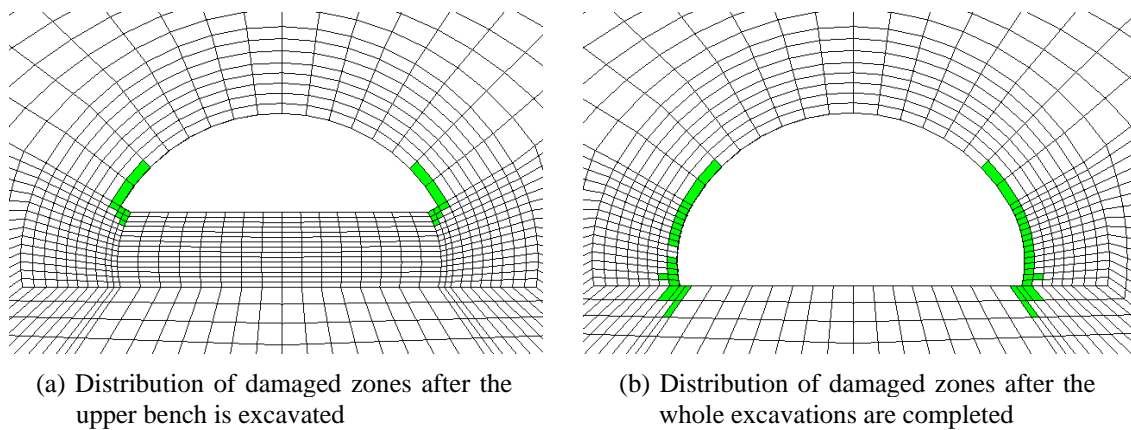


Fig. 10 Distribution of damaged zones in scheme I

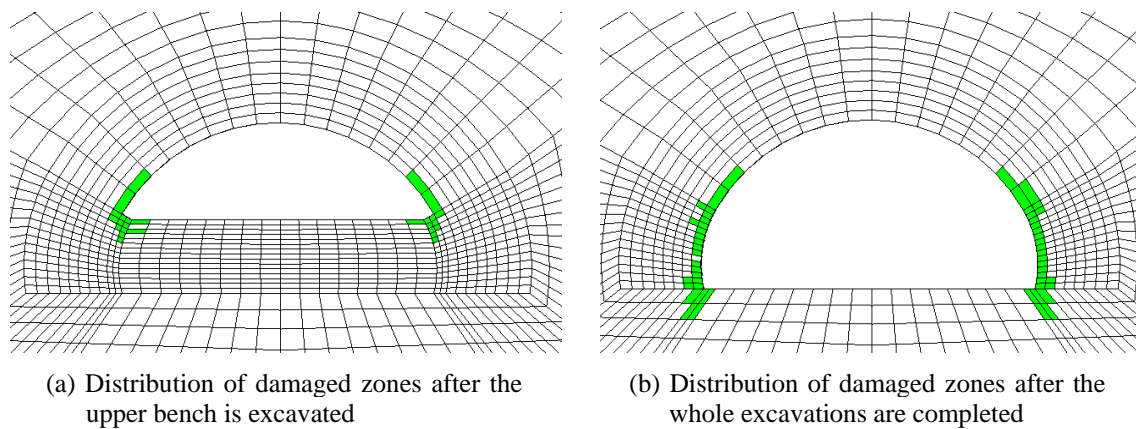


Fig. 11 Distribution of damaged zones in scheme II

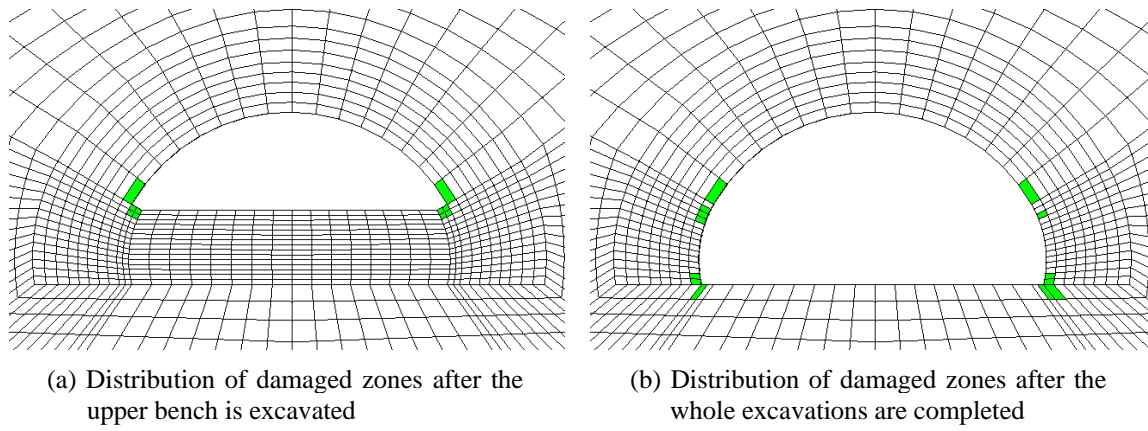


Fig. 12 Distribution of damaged zones in scheme III

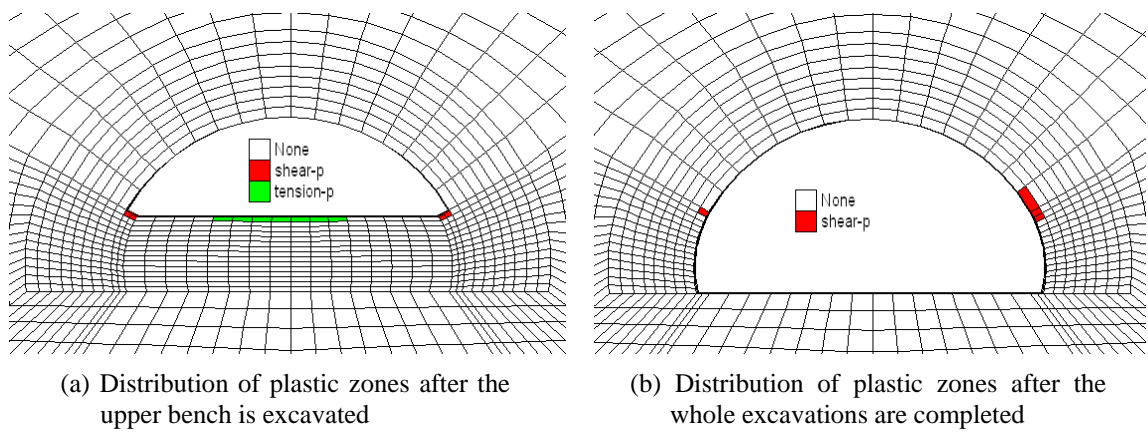


Fig. 13 Distribution of plastic zones obtained by FLAC3D

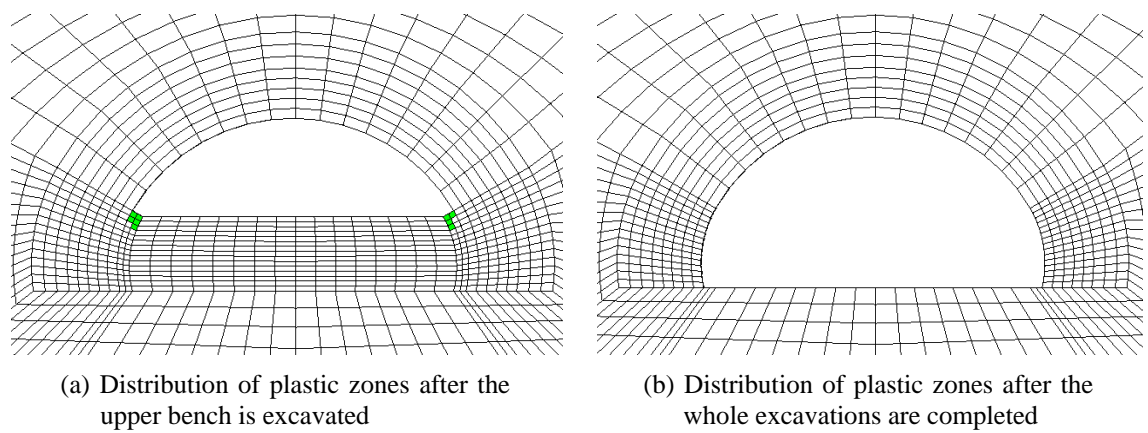


Fig. 14 Distribution of plastic zones in scheme I

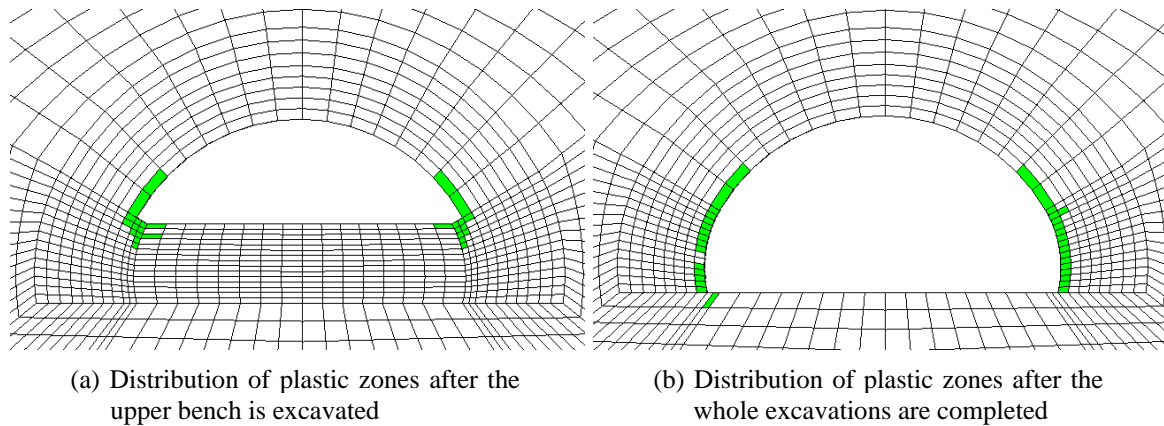


Fig. 15 Distribution of plastic zones in scheme II

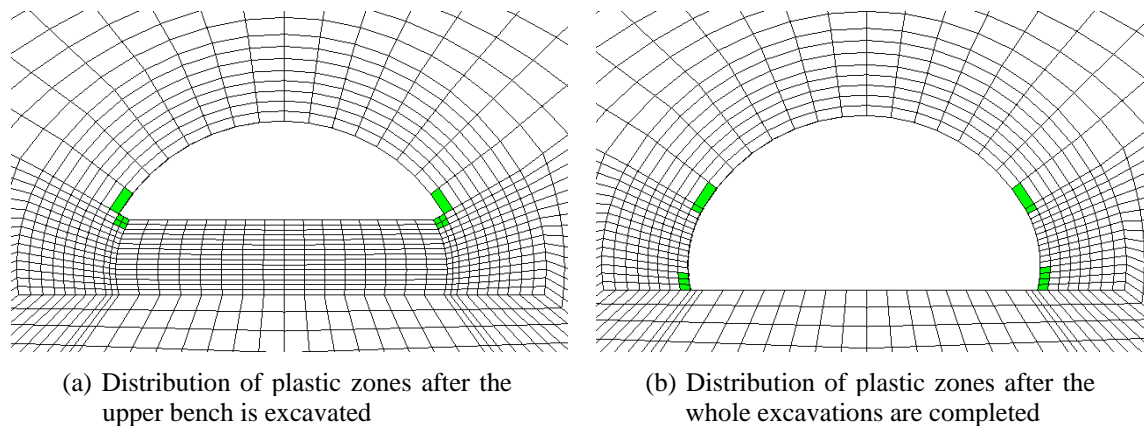


Fig. 16 Distribution of plastic zones in scheme III

4.4.4 Distribution of plastic zones

The distributions of plastic zones obtained by FLAC3D, schemes I, II and III are shown in Figs. 13-16, respectively.

It can be concluded from the above figures on the distribution of plastic zones as below:

- The plastic zones obtained by FLAC3D have similar distribution principle with those in scheme I, and the only difference is that small plastic zones appear in the shoulder area of the arch;
- After considering the damage evolution of the surrounding rock mass, the plastic zones in scheme II is obviously larger than those in scheme III, which demonstrates that the surrounding rock mass is more easily to yield when a smaller damage strain threshold value is adopted;
- All of the plastic zones belong to the shear failure, and the most possible failure positions are located at the shoulder areas of the arch and the floor edge areas.

From the comparative analysis between FLAC3D and the D-FEM code, the numerical results obtained by the D-FEM code can reflect the damage and failure characteristics of the surrounding

rock mass better, especially the distribution of EDZ. The accurate distribution of EDZ would help to provide detailed supporting schemes for the surrounding rock mass. The D-FEM code can consider the damage strain threshold which can be obtained from the in-situ rock mass, therefore the numerical results obtained by the D-FEM code will be in good agreement with the in-situ monitoring results. Additionally, the D-FEM code can provide more constitutive models to adapt to different geo-materials.

5. Conclusions

After analyzing the constitutive models of jointed rock mass proposed by former investigators, an elasto-plastic damage constitutive model for jointed rock mass is newly proposed based on the coupling method considering elasto-plastic and damage theories, and the irreversible thermodynamics theory in this paper. The damage evolution equations expressed with strain are proposed, and the additional nodal force of the damaged element is also presented in this paper. Then, the elasto-plastic damage finite element codes (D-FEM) is programmed, which can numerically simulate the whole excavation process of underground project and perform the structural stability of the surrounding rock mass.

Afterwards, the D-FEM code is used to investigate the surrounding rock mass stability of a big-arch tunnel which belongs to a complex forked tunnel under three different calculating schemes. Meanwhile, FLAC3D is also used in the numerical simulation. The numerical results obtained by FLAC3D are in good agreement with those in scheme I, which verifies the effectiveness of the D-FEM code. From the numerical results in the three schemes, the displacement and plastic zones obviously increase as the damage evolution process is taken into account. The smaller the damage strain threshold value is, the larger the deformation and damaged zones will be. Finally, the most possible failure areas can be determined by analyzing the distributions of plastic and damaged zones in the surrounding rock mass. The D-FEM code proposed in this paper has provided a new approach to study the whole stability in large-scale underground projects.

Acknowledgments

The work was supported by the National Science and Technology Support Program of China (2015BAB07B05) and Major Program of National Scientific Instrument Research (51427804). We would like to express our sincere gratitude to the editor and the two anonymous reviewers for their valuable contributions to this paper.

References

- Bombolakis, E.G. (1968), "Photoelastic study of initial stages of brittle fracture in compression", *Tectonophysics*, **6**(6), 461-473.
- Cai, M. and Kaiser, P.K. (2005), "Assessment of excavation damaged zone using a micromechanics model", *Tunn. Undergr. Sp. Tech.*, **20**(4), 301-310.
- Chen, W.Z., Zhu, W.S. and Shao, J.F. (2004), "Damage coupled time-dependent model of a jointed rock mass and application to large underground cavern excavation", *Int. J. Rock Mech. Min.*, **41**(4), 669-677.
- Drucker, D.C. and Prager, W. (1953), "Soil mechanics and plasticity analysis or limit design", *Q Appl. Math.*, **10**(2), 157-165.

- Haeri, H., Shahriar, K., Marji, M.F. and Moarefvand, P. (2014), "Experimental and numerical study of crack propagation and coalescence in pre-cracked rock-like disks", *Int. J. Rock Mech. Min.*, **67**, 20-28.
- Hoek, E. and Bieniawski, Z.T. (1965), "Brittle fracture propagation in rock under compression", *Int. J. Fract.*, **1**(3), 137-155.
- Hong, K.R. (2015), "State-of-art and prospect of tunnels and underground works in China", *Tunnel Constr.*, **35**(2), 95-107.
- Kachanov, L.M. (1958), "On the creep fracture time", *Izv. Akad. Nauk. USSR Otd. Tekh.*, **8**, 26-31.
- Keats, J.B. and Lawrence, F.P. (1997), "Weibull maximum likelihood parameter estimates with censored data", *J. Qual. Technol.*, **29**, 105-110.
- Krajcinovic, D. (1985), "Continuous damage mechanics revisited: Basic concepts and definitions", *J. Appl. Mech.*, **52**(4), 829-834.
- Kruschwitz, S. and Yaramanci, U. (2004), "Detection and characterization of the disturbed rock zone in claystone with the complex resistivity method", *J. Appl. Geophys.*, **57**(1), 63-79.
- Lee, H. and Jeon, S. (2011), "An experimental and numerical study of fracture coalescence in pre-cracked specimens under uniaxial compression", *Int. J. Solids Struct.*, **48**(6), 979-999.
- Leu, S.Y. (2005), "Convergence analysis and validation of sequential limit analysis of plane-strain problems of the von Mises model with non-linear isotropic hardening", *Int. J. Numer. Meth. Eng.*, **64**(3), 322-334.
- Li, B., Jiang, Y.J., Mizokami, T., Ikusada, K. and Mitani, Y. (2014), "Anisotropic shear behavior of closely jointed rock masses", *Int. J. Rock Mech. Min.*, **71**, 258-271.
- Li, Y., Zhou, H., Zhu, W.S., Li, S.C. and Liu, J. (2015), "Numerical study on crack propagation in brittle jointed rock mass influenced by fracture water pressure", *Materials*, **8**(6), 3364-3376.
- Lin, P., Zhou, Y., Liu, H. and Wang, C. (2013), "Reinforcement design and stability analysis for large-span tailrace bifurcated tunnels with irregular geometry", *Tunn. Undergr. Sp. Tech.*, **38**(9), 189-204.
- Lin, P., Liu, H.Y. and Zhou, W.Y. (2015), "Experimental study on failure behaviour of deep tunnels under high in-situ stresses", *Tunn. Undergr. Sp. Tech.*, **46**, 28-45.
- Liu, W.D. (2015), "Scientific understanding of the belt and road initiative of China and related research themes", *Prog. Geogr.*, **34**(5), 538-544.
- Liu, H.Y. and Yuan, X.P. (2014), "A damage constitutive model for rock mass with persistent joints considering joint shear strength", *Can. Geotech. J.*, **52**(8), 1136-1143.
- Liu, H.Y., Small, J.C., Carter, J.P. and Williams, D.J. (2009), "Effects of tunnelling on existing support systems of perpendicularly crossing tunnels", *Comput. Geotech.*, **36**(5), 880-894.
- Ma, J., Sun, S.Z., Zhao, W.Y., Wang, L., Ma, Y., Liu, H., Zhang, W.W., Chen, H.Y., Chen, L., Wei, Y.W. and Ye, F. (2015), "Review on China's tunnel engineering research: 2015", *China J. Highway Transport*, **28**(5), 1-65.
- Mazars, J. and Pijaudier-Cabot, G. (1989), "Continuum damage theory-application to concrete", *J. Eng. Mech.-ASCE*, **115**(2), 345-365.
- Ng, C.W.W., Boonyarak, T. and Mašin, D. (2013), "Three-dimensional centrifuge and numerical modeling of the interaction between perpendicularly crossing tunnels", *Can. Geotech. J.*, **50**(9), 935-946.
- Qin, Y.P. (2001), "Discussion on damage mechanics model and constitutive equation of rock", *Chin. J. Rock Mech. Eng.*, **20**(4), 560-562.
- Sato, T., Kikuchi, T. and Sugihara, K. (2000), "In-situ experiments on an excavation disturbed zone induced by mechanical excavation in Neogene sedimentary rock at Tono mine, central Japan", *Eng. Geol.*, **56**(1-2), 97-108.
- Schuster, K., Alheid, H.J. and Böddener, D. (2001), "Seismic investigation of the Excavation damaged zone in Opalinus Clay", *Eng. Geol.*, **61**(2-3), 189-197.
- Sheng, Q., Yue, Z.Q., Lee, C.F., Tham, L.G. and Zhou, H. (2002), "Estimation the excavation disturbed zone in the permanent shiplock slopes of the Three Gorges Project, China", *Int. J. Rock Mech. Min.*, **39**(2), 165-184.
- SHIDI (2004), The reasonable layout and surrounding rock stability research of Baziling forked tunnel; The Second Highway Investigation and Design Institute (SHIDI), Report, Wuhan, China.
- Shih, V. (2004), "Development, the second time around: The political logic of developing western China", *J.*

- East Asian Stud.*, **4**(3), 427-451.
- Singh, M. and Singh, B. (2012), "Modified Mohr-Coulomb criterion for non-linear triaxial and polyaxial strength of jointed rocks", *Int. J. Rock Mech. Min. Sci.*, **51**, 43-52.
- Taiebat, H.A. and Carter, J.P. (2008), "Flow rule effects in the Tresca model", *Comput. Geotech.*, **35**(3), 500-503.
- Tang, C.A. (1997), "Numerical simulation of progressive rock failure and associated seismicity", *Int. J. Rock Mech. Min.*, **34**(2), 249-261.
- Tecplot, Inc. (2013), Tecplot 360 User's Manual, Tecplot Inc., Bellevue, WA, USA.
- Voyiadjis, G.Z. and Park, T. (1999), "The kinematics of damage for finite-strain elasto-plastic solids", *Int. J. Eng. Sci.*, **37**(7), 803-830.
- Wang, H.W., Jiang, Y.D., Xue, S., Shen, B.T., Wang, C., Lv, J.G. and Yang, T. (2015), "Assessment of excavation damaged zone around roadways under dynamic pressure induced by an active mining process", *Int. J. Rock Mech. Min.*, **77**, 265-277.
- Weibull, W. (1951), "A statistical distribution function of wide applicability", *J. Appl. Mech.*, **103**, 293-297.
- Wu, F.Q., Liu, J.Y., Liu, T., Zhuang, H.Z. and Yan, C.G. (2009), "A method for assessment of excavation damaged zone (EDZ) of a rock mass and its application to a dam foundation case", *Eng. Geol.*, **104**(3-4), 254-262.
- Zhu, W.S., Zhang, Q.Y., Li, S.C. and Lee, C.F. (2003), "Brittle elastoplastic damage constitutive model for jointed Rock masses and computation concerning bolt-reinforcement", *Int. J. Damage Mech.*, **12**(1), 65-84.
- Zhu, W.S., Li, Y., Li, S.C., Wang, S.G. and Zhang, Q.B. (2011), "Quasi-three-dimensional physical model tests on a cavern complex under high in-situ stresses", *Int. J. Rock Mech. Min.*, **48**(2), 199-209.
- Zienkiewicz, O.C., Chang, C.T. and Bettess, P. (1980), "Drained, undrained, consolidating dynamic behaviour assumptions in soils", *Géotechnique*, **30**(4), 385-395.